Indirect Path Detection Based on Wireless Propagation Measurements

Junyang Shen, *Student Member, IEEE*, and Andreas F. Molisch, *Fellow, IEEE*

***Abstract*—An important prerequisite for precise localization, such as in radar systems, is to discern "direct paths" (DP), i.e., multipath components (MPCs) where the signal propagates directly between the target and the localization system nodes (transmitters or receivers), from indirect paths (IPs). This paper describes how to distinguish between DPs and IPs purely based on measurements of observable propagation parameters, namely the time of arrival (TOA), direction of departure (DOD), and direction of arrival (DOA). Any combination of two of those parameters allow the computation of a reflection point, and - in the absence of noise - the points computed from the different combinations are consistent in the case of a DP. In the presence of noise, the computed points deviate from each other, and we establish rules for how large this deviation might be to consider a path an IP. Several different decision rules are discussed and compared. The paper derives closed-form equations for these decision criteria and the resulting performance. The situations when the proposed decision rules do not work well are also studied. Simulation results show that under common localization scenarios employing ultrawideband signals, the proposed algorithms can effectively detect IPs and significantly improve localization accuracy.**

***Index Terms*—TOA, DOD, DOA, indirect path detection.**

I. Introduction

RADIO positioning technologies have recently received a large amount of attention for various applications, such as surveillance, patient monitoring, survivor localization in emergency rescue operations, logistics, and node localization in sensor networks. Specific techniques range from GPS, which is ubiquitous for outdoor applications, to indoor positioning systems based on ultra-wide-band signals [2], [3]. The latter have drawn great attention because they can achieve highly accurate (millimeter level) target location estimates [4], [5]. The bounds on UWB based localization accuracy have been studied in [6] and [7].

The target to be localized can be either "active", transmitting/receiving signals, or "passive", only reflecting signals transmitted by a separate source (and received by separate receivers). Active target positioning scenarios include cell phone location estimation or wireless sensor positioning in the IEEE 802.15.4a Wireless Sensor Networks (WSNs) [8]. [9] has developed a special concept of active localization to use cooperation between several targets (agents) to improve localization accuracy. The passive target positioning scenario is typical in applications such as survivor rescue, anti-theft surveillance, and automated environment mapping. Radar is also a "passive" localization technology, which has been studied for many years [10]–[12]. In addition, the "passive" localization was recently shown to be a promising technology for cancer detection [13]. For ease of notation, this paper will concentrate on passive localization techniques, though many of the results are useful in active localization as well.

Radio positioning technologies employ the measured characteristics (such as time of arrival TOA, direction of departure DOD, and direction of arrival DOA) of multipath components (MPCs) propagating between target and the nodes of the localization system (the nodes can be transmitters or receivers). For the subsequent discussion, it is useful to distinguish between the direct path (DP), i.e., a MPC where the signal propagates directly between the target and the localization system nodes and the indirect paths (IPs), where the signal interacts with one or more objects/obstacles in addition to the target and system nodes. For an active localization system, an indirect path is any non-line-of-sight (NLOS) path.

Extensive studies [14]–[16], show that IPs lead to worse localization accuracy, especially for precise localization. This is because IPs create biases in the DOD, TOA and TOA estimates, resulting in erroneous estimates of target location. More importantly, the localization error from IPs can not be mitigated by averaging over multiple measurements - in contrast to noise-induced localization errors.

To combat the negative effects of IPs in *active* localization systems, various techniques have been proposed in the literature. They can be divided into two categories, IP *mitigation* and IP *detection* [17]. IP mitigation attempts to alleviate or counter the bias of channel parameters introduced by IPs [18]–[23], while IP detection attempts to differentiate DPs and IPs so that channel parameters of IPs are not used in the DP based positioning algorithms [24]–[29]. Performance evaluation and comparison of existing IP detection schemes were performed in [30]. [23] practically studied the IP detection problem, and proposed a maximum a posteriori probability detection method based on root mean square delay, kurtosis and maximum amplitude. In [24], the IP detection was performed by analysing multipath channel statistics such as the kurtosis, the mean excess delay, and the root-mean-square delay. [25] employed the energy statistics of direct-path pulse and certain delay statistics for IP detection. The delay between the first and the strongest impulse was employed in [26]. In [27], the IP detection was based on testing whether angle estimates were matched between transmitter and receiver, or based on

Manuscript received January 18, 2012; revised June 25 and August 31, 2012; accepted October 22, 2012. The associate editor coordinating the review of this paper and approving it for publication was M. Bhatnagar.

The authors are with the Ming Hsieh Department of Electrical Engineering, Viterbi School of Engineering, University of Southern California (e-mail: {junyangs, molisch}@usc.edu).

Part of this paper was presented in [1] IEEE International Conference on Ultra-Wideband (ICUWB), 2012.

Digital Object Identifier 10.1109/TWC.2012.112012.120104

whether signal travel range matched power decay. [28] utilized the estimated TOA and Received Signal Strength (RSS) for IP detection. [29] studied characterization of differences in the channel pulse responses under IP and DP conditions, and proposed non-parametric machine learning techniques to perform IP identification. Thus, there is a wealth of IP detection scheme in the literature; however, they rely on features such as delay spread to discern IPs, which in turn rely on the environment, which the system might not know with sufficient accuracy.

The situation is fundamentally different in *passive* localization systems, where an IP is a path that has interactions with one or more objects/obstacles *in addition to* the target. In many localization scenarios, especially indoor environments, there are rich IPs during signal propagation. In other words, in passive localization systems, the DP implies a single-reflection process (at the target), while IPs undergo multiple reflections (at non-target reflectors). The detection of IP in passive localization requires the discrimination between single-reflections and multiple-reflections; a task that is fundamentally different from the detection of line-of-sight paths encountered in active systems. Most existing IP detection methods for active targets, as described above, are essentially based on the fact that signal characteristics change after reflection in NLOS paths. Thus, they are not expected to work well for passive target since reflection happens in both IP and NP paths for passive localization.

To fill this gap, this paper focuses on IP detection for precise passive target localization. We assume that the DOD, DOA and TOA measurements are available as triplets, from channel sounding algorithms such as SAGE [31] or RiMax [32], [33]. Note that to obtain the DOD and DOA information, the localization system needs antenna arrays or directional antennas. We propose a new TDAJ (TOA, DOD, DOA joint) IP detection scheme, based on such measurements. TDAJ eliminates the dependence on "tuning parameters" such as "typical" received power and delay spread. The only information needed by TDAJ is the statistical distributions of DOD, DOA and TOA measurement errors, which can be easily obtained from the measurements themselves. For some models of DOD, DOA and TOA errors, such as Gaussian distribution, only a small number of parameters (variance) need to be known.

The principle of the algorithm is as follows: if there were no measurement errors, any DP would have self-consistent parameters. By this we mean that the three intersections obtained from the pairs of measured parameters (DOA line with the TOA ellipse, DOD line with the TOA ellipse, and DOA line with the DOD line) are at the same location. In the presence of measurement errors, the decision variables of the Neyman-Pearson (NP) test are the differences between two of the three intersections in x or y coordinates: only if this difference lies below a certain threshold, the algorithm judges the path to be a DP. The TDAJ algorithm is developed under the NP criterion so it is able to achieve desired probability of false alarm (PF) and maximize the probability of detection (PD).

Although the TDAJ is designed for passive target localization, its principle can be also used for active target locations. Single-reflection paths can act as "virtual sources" according to the image principle [34] in active systems, and thus make localization in the presence of multipath propagation *more* accurate than without multipath [35]. To employ the "virtual sources" to improve localization accuracy, we still need to discern the single reflection and the multiple reflector paths.

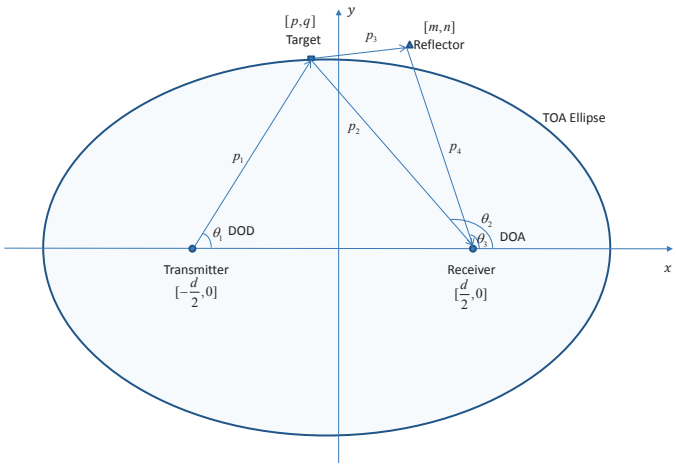

Fig. 1. Illustration of DPs and IPs.

Particularly, we made following contributions in this paper:

- Propose the idea of IP detection based on the differences of the three geographical intersections of DOD, DOA and TOA measurements in x or y coordinates. This is a more general form of an idea presented in [36].
- Prove that for small errors of DOD, DOA and TOA measurements, the six decision variables (differences between the three intersections) are the linear transformations of the measurement errors of DOD, DOA and TOA. Then, the distributions of the decision variables and the thresholds to achieve a given PF are obtained.
- Study the relationship between the six decision variables in DPs, and prove that they are linearly dependent as summarized in *Theorem 1*.
- Derive the closed-form expressions of PD given an expected PF. Further define a "safe region" which better evaluates the impact of IPs on localization accuracy.
- Investigate the situations when the decision rules do not work as expected and compare the performances of various decision rules via simulations. Simulations also show significant localization accuracy improvement by the TDAJ algorithm.

The remainder of this paper is organized as follows. Section II presents the system model. The principle of TDAJ is presented in Section III. In Section IV, we study the distribution of the decision variable, evaluations of PF and PD, the "blind spots" of different rules and the outage probability. The detailed procedure of TDAJ algorithm is shown in Section V. The simulation results are shown in Section VI and the conclusions are drawn in Section VII. In the remainder of this paper, we let $\bar{\bullet}$ denote the true value, $\hat{\bullet}$ denote the estimated or measured value, and $\Delta\bullet = \hat{\bullet} - \bar{\bullet}$.

II. System Model

In this section, we present the system model, assumptions and discuss the importance of IP detection for precise localization systems.

For simplicity, we consider a two dimensional scenario, as shown in Fig. 1, though extension to three dimensions is straightforward. There is one transmitter at $[-\frac{d}{2}, 0]$, and one receiver at $[\frac{d}{2}, 0]$. We assume that estimates of the tuplets of DOA, DOD, and TOA are available, for all MPCs, from array measurements at the TX and RX. Measurement methods and algorithms for the extraction of these MPC parameters (with automatic pairing) have been discussed, e.g., in [32], [33], [37]. Without restriction of generality, we consider in the following a single MPC, for which we determine whether it is a DP or IP. The target is located at $[p, q]$ and a possible obstacle (which could give rise to additional interactions) is at $[m, n]$. Then the DP is associated with a tuplet $(\theta_1; \theta_2; p_1+p_2)$, while an IP corresponds to $(\theta_1; \theta_3; p_1 + p_3 + p_4)$.

Note that in the above example, the reflector is on the way from target to receiver. The obstacle might be positioned such that interaction with it occurs "on the way" from TX to target; this case can be treated completely analogously. Furthermore, interactions with multiple reflectors (obstacles) are possible, and could be included in our model; however, for the sake of simplicity, we restrict our attention to the case depicted in Fig. 1.

The localization errors happen due to either the measurement noise or the IPs:

- Measurement noise leads to errors of DOD, DOA and TOA estimates and finally errors of target location estimates. The errors from measurement noise are zero mean, and averaging over multiple runs could mitigate the error of localization. Irrespective of possible averaging, we assume in the following that the errors of DOD, DOA and TOA measurements due to noise are small, and their statistical distributions are known.
- IPs should not be used for localization generally [1], since the association between TOA/DOD/DOA and reflector locations is not bijective. Erroneously using IPs leads to biases to DOD, DOA and TOA estimates, also resulting in errors of target location estimates. Moreover, the errors of localization cannot be decreased by averaging.

The IP detection is particularly important for precise localization systems based on ultra-wideband signals. This is because the errors of DOD, DOA and TOA measurements due to noise are small compared with those due to IPs. For instance, [33] and [38], [39] show that in an anechoic chamber, with ultra-wide-band signals (2-8 GHz) and sophisticated channel sounding techniques (RIMAX [33]), the standard deviation of the signal travel range (proportional to TOA) can be less than 0.5 cm, and the standard deviations of DOD and DOA measurements can be less than 0.5 degree. In [40], with 1.5 GHz bandwidth signals, ranging errors of about 10 cm and angular errors of about 1 degree are achieved. In these two examples, the errors are due to noise. Regarding errors due to IPs, the range estimate bias $(p_3 + p_4 - p_2)$ and angle estimate bias $(\theta_3 - \theta_2)$ can easily be on the orders of meters, and tens of degrees, respectively. Thus, IPs severely degrade localization accuracy, especially in indoor environments, where a multitude of reflectors such as walls and tables exist. To improve the localization accuracy, it is vital to first identify the IPs. Then, the IPs can either be discarded or combined with the DPs for localization according to the methods described in [23].

[1] though, see [23], as discussed below.

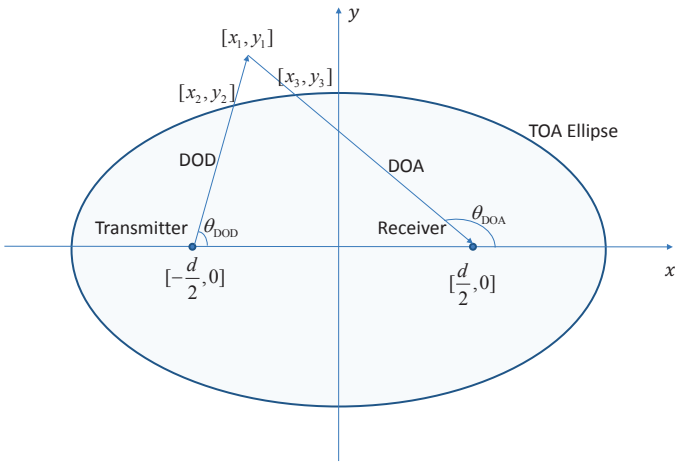

Fig. 2. Illustration of TOA, DOA and DOD joint location estimation.

III. IP Detection Scheme based on Differences of Intersections

In this section, we present the principle of the proposed IP detection scheme based on differences of intersections of DOD/DOA, DOD/TOA and DOA/TOA in x or y coordinates. The basic idea is that if DOD, DOA and TOA measurements are consistent, the three intersections from them would be close with each other. Otherwise, the three intersections would be far from each other.

As shown in Fig. 2, the coordinates of reflection points giving a specific DOD, DOA, or TOA, respectively, can be written as follows,

$$\text{DOD:} \qquad y = \tan(\theta_{\text{DOD}})(x + \frac{d}{2}), \tag{1}$$

$$\text{DOA:} \qquad y = \tan(\theta_{\text{DOA}})(x - \frac{d}{2}), \tag{2}$$

$$\text{TOA:} \qquad \frac{x^2}{(\frac{l}{2})^2} + \frac{y^2}{(\frac{l}{2})^2 - (\frac{d}{2})^2} = 1. \tag{3}$$

Note that $l = c_0 \cdot \text{TOA}$, where c_0 is the speed of light and TOA is the signal travel time. (1) and (2) denote two lines and (3) is an ellipse.

Throughout this paper, we assume there is no ambiguity in the DOD and DOA estimation: the system can effectively differentiate θ_{DOD} and $\theta_{\text{DOD}} \pm \pi$, θ_{DOA} and $\theta_{\text{DOA}} \pm \pi$. Without loss of generality, we assume that $0 \leq \theta_{\text{DOD}} \leq \pi$ and $0 \leq \theta_{\text{DOA}} \leq \pi$. Practically, the ambiguity can be removed by combining the DOA estimates from several receivers: the correct DOA lines from every receiver should point to the correct target location. Other methods such as using rough prior information of the target location can also remove the DOD and DOA ambiguity.

$$\begin{aligned} p_{f,fr}^{K} &= \text{Prob } ((\text{Number of } |\lambda_i| \text{ larger than } \delta_i) > K \,\big|\, \text{The path is a DP}), \\ p_{d,fr}^{K} &= \text{Prob } ((\text{Number of } |\lambda_i| \text{ larger than } \delta_i) > K \,\big|\, \text{The path is an IP}). \end{aligned} \tag{4}$$

Due to measurement errors or IPs, DOD, DOA and TOA intersect at three points instead of one. Let $[\hat{x}_1, \hat{y}_1]$, $[\hat{x}_2, \hat{y}_2]$ and $[\hat{x}_3, \hat{y}_3]$ denote the locations of intersections of DOD/DOA, DOD/TOA, DOA/TOA. Then, there are six difference observations of the three intersections as follows:

$$\hat{\boldsymbol{\lambda}} = \begin{bmatrix} \lambda_1 \\ \lambda_2 \\ \lambda_3 \\ \lambda_4 \\ \lambda_5 \\ \lambda_6 \end{bmatrix} = \begin{bmatrix} \hat{x}_1 - \hat{x}_2 \\ \hat{y}_1 - \hat{y}_2 \\ \hat{x}_1 - \hat{x}_3 \\ \hat{y}_1 - \hat{y}_3 \\ \hat{x}_2 - \hat{x}_3 \\ \hat{y}_2 - \hat{y}_3 \end{bmatrix} \tag{5}$$

Since there are 6 observations, the TDAJ IP detection can be based on individual rule or fusion rule:

- Individual rule: the final decision is based solely on one λ_i: if $|\lambda_i|$ is larger than a threshold δ_i, TDAJ claims an IP, otherwise, claims a DP.
- Fusion rule: The final decision is based on a fusion of the six observations: if the number of $|\lambda_i|$ larger than a threshold δ_i $(i = 1, 2, ..., 6)$ is larger than K $(K = 0, 1, ..., 5)$, the detection algorithm claims that it is an IP, otherwise, the detection algorithm claims that it is a DP.

To evaluate the IP detection performance, the probability of false alarm (PF) and probability of detection (PD) are:

$$\begin{aligned} P_f &= \text{Prob (The algorithm claims an IP} \,\big|\, \text{The path is a DP}), \\ P_d &= \text{Prob (The algorithm claims an IP} \,\big|\, \text{The path is an IP}). \end{aligned} \tag{6}$$

For each individual measurement λ_i, PF and PD can be evaluated as follows:

$$\begin{aligned} p_f^i &= \text{Prob } (|\lambda_i| > \delta_i \,\big|\, \text{The path is a DP}), \\ p_d^i &= \text{Prob } (|\lambda_i| > \delta_i \,\big|\, \text{The path is an IP}). \end{aligned} \tag{7}$$

For fusion rule, the decision strategy is shown in (4).

where the subscript "fr" denotes the fusion rule, and the superscript K is a parameter characterizing the fusion rule. Because a DP means no reflector, the PF is independent of the locations of obstacles/reflectors while the PD is not. In most situations, the locations of the reflectors are unknown, thus, an ideal strategy of TDAJ scheme is based on the Neyman-Pearson rule [41] to choose a threshold δ to achieve a desired PF, and at the same time maximize PD.

IV. Distribution of Decision Variables and Evaluations of P_f and P_d

In this section, we study the decision variables λ_i and then present the evaluations of PF and PD. To better evaluate the impact of IPs on localization, we define a "safe region" and outage probability. We also investigate the situations where the TDAJ algorithm does not work well.

Let the true/mean values of the locations of the DOD/DOA, DOD/TOA, DOA/TOA intersections be $[\bar{x}_1, \bar{y}_1]$, $[\bar{x}_2, \bar{y}_2]$ and $[\bar{x}_3, \bar{y}_3]$, respectively. The noise induced deviations from the means of the locations of the three intersections are denoted by

$$[\Delta x_k,\ \Delta y_k] = [\hat{x}_k - \bar{x}_k,\ \hat{y}_k - \bar{y}_k], \quad k = 1, 2, 3, \tag{8}$$

where $[\hat{x}_1, \hat{y}_1]$, $[\hat{x}_2, \hat{y}_2]$ and $[\hat{x}_3, \hat{y}_3]$ are the measured locations of intersections of DOD/DOA, DOD/TOA, DOA/TOA. For notational convenience, we define $\mu_1 = \theta_{\text{DOA}}$, $\mu_2 = \theta_{\text{DOD}}$ and $\mu_3 = l$. Taking the derivatives of (1) - (3) with respect to μ_1, μ_2 and μ_3, the deviations of x_k, y_k and μ_k satisfy

$$a_k^k \Delta x_k + b_k^k \Delta y_k + c_k^k \Delta \mu_k = 0, \tag{9}$$

$$a_{k+1,\text{mod}\,3}^k \Delta x_k + b_{k+1,\text{mod}\,3}^k \Delta y_k + c_{k+1,\text{mod}\,3}^k \Delta \mu_{k+1,\text{mod}\,3} = 0, \tag{10}$$

where $k = 1, 2, 3$, mod3 denotes taking the index modulo 3, and

$$\begin{aligned} &a_1^k = \tan\bar{\mu}_1, \quad b_1^k = -1, && c_1^k = \frac{\bar{x}_k - \frac{d}{2}}{\cos^2(\bar{\mu}_1)}, \\ &a_2^k = \tan\bar{\mu}_2, \quad b_2^k = -1, && c_2^k = \frac{\bar{x}_k + \frac{d}{2}}{\cos^2(\bar{\mu}_2)}, \\ &a_3^k = \frac{2\bar{x}_k}{\bar{\mu}_3^2}, \quad b_3^k = \frac{2\bar{y}_k}{\bar{\mu}_3^2 - d^2}, && c_3^k = -2\Big(\frac{\bar{x}_k^2}{\bar{\mu}_3^3} - \frac{\bar{y}_k^2 \bar{\mu}_3}{(\bar{\mu}_3^2 - d^2)^2}\Big). \end{aligned} \tag{11}$$

Here a, b and c with superscript k are parameters for the intersection $[x_k, y_k]$. We actually use derivatives (first order Taylor expansion) to approximate the noise induced errors. Note that these above parameters depend on $[\bar{x}_k, \bar{y}_k]$ and $\bar{\mu}_k$, $k = 1, 2, 3$, which are actually unknown. We assume that they are known for the purpose of analyzing the distribution of decision variable λ_i and the evaluation of PD and PF. In Section V, we will discuss the TDAJ scheme based on estimates of these variables.

For notational convenience, we can define the following quantities:

$$\alpha = a_1^1 b_2^1 - a_2^1 b_1^1, \tag{12a}$$

$$\beta = a_2^2 b_3^2 - a_3^2 b_2^2, \tag{12b}$$

$$\gamma = a_3^3 b_1^3 - a_1^3 b_3^3. \tag{12c}$$

By solving (9) and (10) for different k, we can obtain

$$\boldsymbol{\varepsilon} = \begin{bmatrix} \Delta x_1 - \Delta x_2 \\ \Delta y_1 - \Delta y_2 \\ \Delta x_1 - \Delta x_3 \\ \Delta y_1 - \Delta y_3 \\ \Delta x_2 - \Delta x_3 \\ \Delta y_2 - \Delta y_3 \end{bmatrix} = \mathbf{W} \boldsymbol{\Delta\mu}. \tag{13}$$

where

$$\mathbf{W} = \begin{bmatrix} -\frac{c_1^1 b_2^1}{\alpha} & \frac{c_2^1 b_1^1}{\alpha} + \frac{c_2^2 b_3^2}{\beta} & -\frac{b_2^2 c_3^2}{\beta} \\ \frac{a_2^1 c_1^1}{\alpha} & -\frac{a_1^1 c_2^1}{\alpha} - \frac{c_2^2 a_3^2}{\beta} & \frac{a_2^2 c_3^2}{\beta} \\ -\frac{b_2^1 c_1^1}{\alpha} - \frac{b_3^3 c_1^3}{\gamma} & \frac{b_1^1 c_2^1}{\alpha} & \frac{b_1^3 c_3^3}{\gamma} \\ \frac{a_2^1 c_1^1}{\alpha} + \frac{c_3^3 a_3^3}{\gamma} & -\frac{a_1^1 c_2^1}{\alpha} & -\frac{a_1^3 c_3^3}{\gamma} \\ -\frac{b_3^3 c_1^3}{\gamma} & -\frac{b_2^2 c_2^2}{\beta} & \frac{b_2^2 c_3^2}{\beta} + \frac{b_1^3 c_3^3}{\gamma} \\ \frac{a_3^3 c_1^3}{\gamma} & \frac{a_3^2 c_2^2}{\beta} & -\frac{a_2^2 c_3^2}{\beta} - \frac{a_1^3 c_3^3}{\gamma} \end{bmatrix}, \tag{14}$$

$$\boldsymbol{\Delta\mu} = [\Delta\mu_1, \Delta\mu_2, \Delta\mu_3]^T. \tag{15}$$

According to (5) and (13), we can evaluate the observations of differences by

$$\hat{\boldsymbol{\lambda}} = \bar{\boldsymbol{\lambda}} + \boldsymbol{\varepsilon}, \tag{16}$$

where $\hat{\boldsymbol{\lambda}} = [\hat{x}_1 - \hat{x}_2, \hat{y}_1 - \hat{y}_2, \hat{x}_1 - \hat{x}_3, \hat{y}_1 - \hat{y}_3, \hat{x}_2 - \hat{x}_3, \hat{y}_2 - \hat{y}_3]^T$ and $\bar{\boldsymbol{\lambda}} = [\bar{x}_1 - \bar{x}_2, \bar{y}_1 - \bar{y}_2, \bar{x}_1 - \bar{x}_3, \bar{y}_1 - \hat{y}_3, \bar{x}_2 - \bar{x}_3, \bar{y}_2 - \bar{y}_3]^T$ are the mean of $\hat{\boldsymbol{\lambda}}$.

Discussions: *It can be easily proven that* $\bar{\lambda}_i = 0$ *in the case of DPs when* $\bar{x}_1 = \bar{x}_2 = \bar{x}_3$ *and* $\bar{y}_2 = \bar{y}_2 = \bar{y}_3$*, while* $\bar{\lambda}_i \neq 0$ *in the case of IPs.*

In the following, the evaluations of p_f^i and p_d^i are presented.

A. Distribution of λ_i in DPs and evaluation of p_f^i

In the case of DPs, a_j^k, b_j^k, c_j^k $(j = 1, 2, 3)$ and $[\bar{x}_k, \bar{y}_k]$ have the same values for different k, and $\bar{\lambda}_i = 0$ with $i = 1, 2, ..., 6$. For notational convenience, let $\hat{\lambda}_i^{DP}$ denote the value of λ_i in the case of DPs and $\hat{\boldsymbol{\lambda}}^{\boldsymbol{DP}} = [\hat{\lambda}_1^{DP}, \hat{\lambda}_2^{DP}, ..., \hat{\lambda}_6^{DP}]^T$. Also, let $a_j = a_j^k$, $b_j = b_j^k$ and $c_j = c_j^k$ for $j = 1, 2, 3$. Then, we can show the relations between the 6 difference observations in the following theorem.

Theorem 1: In the case of DP, the six difference observations $\hat{\lambda}_i$ $(i = 1, 2, ..., 6)$ are linearly dependent:

$$\omega_1\hat{\lambda}_1^{DP} = \omega_2\hat{\lambda}_2^{DP} = \omega_3\hat{\lambda}_3^{DP} = \omega_4\hat{\lambda}_4^{DP} = \omega_5\hat{\lambda}_5^{DP} = \omega_6\hat{\lambda}_6^{DP}, \tag{17}$$

where

$$\omega_1 = 1, \qquad \omega_2 = -\frac{b_2}{a_2}, \qquad \omega_3 = -\frac{b_2\gamma^{DP}}{b_1\beta^{DP}},$$
$$\omega_4 = \frac{b_2\gamma^{DP}}{a_1\beta^{DP}}, \qquad \omega_5 = \frac{b_2\gamma^{DP}}{b_3\alpha^{DP}}, \qquad \omega_6 = -\frac{b_2\gamma^{DP}}{a_3\alpha^{DP}},$$

with

$$\alpha^{DP} = a_1b_2 - a_2b_1, \tag{18a}$$
$$\beta^{DP} = a_2b_3 - a_3b_2, \tag{18b}$$
$$\gamma^{DP} = a_3b_1 - a_1b_3. \tag{18c}$$

Proof: Please refer to the Appendix. ■

Theorem 1 implies that any one of the six observations contains all the information to evaluate the level of consistency between DOD, DOA and TOA measurements. Thus, we have

$$P_f = p_f^i, \qquad i = 1, 2, ..., 6.$$

An interpretation of *Theorem 1* is illustrated in Fig. 3. The difference observations λ_i $(i = 1, 2, ..., 6)$ are also shown in the figure. The TDJA essentially employs linear approximations to set up the relations between the changing of three intersections $([x_j, y_j],\ j = 1, 2, 3.)$ and μ_1, μ_2 and μ_3 as shown in (9). Thus, we treat the DOD, DOA and TOA as three lines shown in Fig. 3. The changing of the three lines generates a triangle. The shape of the triangle is determined by the absolute DOA, DOD, and TOA, and only the size (scaling) of the triangle depends on the error. Thus, the triangle is completely defined, and all the values of λ_i can be calculated, if any one of the λ_i is known. This interpretation also allows to show easily that the method in our recent conference paper [36] is actually a special case of the TDAJ method in this paper. The decision variable in [36] is the distance from DOD/DOA intersection to TOA ellipse. Based on the result of *Theorem 1*, it is linearly dependent with λ_i in case of DPs.

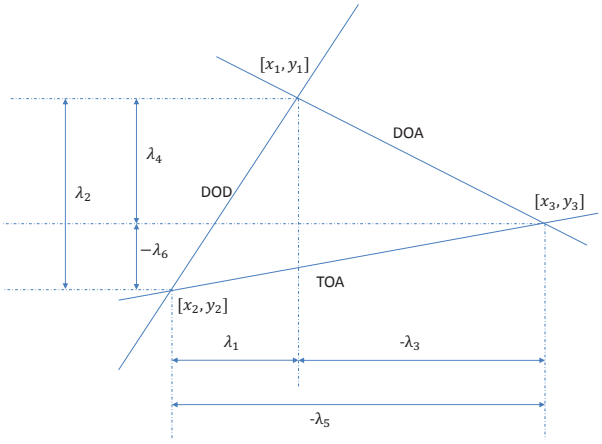

Fig. 3. Interpretation of *Theorem 1*.

Since $\bar{\lambda}_i = 0$ in the case of DP, from (14) and (16), it follows that λ_i^{DP} is evaluated by

$$\lambda_i^{DP} = W_{i,1}\Delta\mu_1 + W_{i,2}\Delta\mu_2 + W_{i,3}\Delta\mu_3, \tag{19}$$

where $W_{i,j}$ is the entry of $\mathbf{W}$ in (14) on the ith row and the jth column.

Assume that the probability density functions of DOA, DOD and TOA measurement errors $f_{\Delta\mu_1}(x)$, $f_{\Delta\mu_2}(x)$ and $f_{\mu 3}(x)$ are known. Then, let $\Delta\mu_1^i = W_{i,1}\Delta\mu_1$, $\Delta\mu_2^i = W_{i,2}\Delta\mu_2$ and $\Delta\mu_3^i = W_{i,3}\Delta\mu_3$, the distributions of $\Delta\mu_1^i, \Delta\mu_2^i, \Delta\mu_3^i$ are

$$g_{\Delta\mu_1^i}^{DP}(y) = \frac{1}{|W_{i,1}|} f_{\Delta\mu_1}\Big(\frac{y}{W_{i,1}}\Big), \tag{20}$$

$$g_{\Delta\mu_2^i}^{DP}(y) = \frac{1}{|W_{i,2}|} f_{\Delta\mu_2}\Big(\frac{y}{W_{i,2}}\Big), \tag{21}$$

$$g_{\Delta\mu_3^i}^{DP}(y) = \frac{1}{|W_{i,3}|} f_{\Delta\mu_3}\Big(\frac{y}{W_{i,3}}\Big). \tag{22}$$

Then, the distribution of λ_i^{DP} is

$$f_{\lambda_i}^{DP}(z) = (g_{\Delta\mu_1^i}^{DP} * g_{\Delta\mu_2^i}^{DP} * g_{\Delta\mu_3^i}^{DP})(z). \tag{23}$$

where $*$ denotes the convolution operation.

Particularly, if $\Delta\mu_1$, $\Delta\mu_2$ and $\Delta\mu_3$ are Gaussian distributed with variances σ_1^2, σ_2^2 and σ_3^2, respectively, the decision variable λ_i^{DP} is also a Gaussian random variable with variance

$$\sigma_{\lambda_i^{DP}}^2 = (W_{i,1}\sigma_1)^2 + (W_{i,2}\sigma_2)^2 + (W_{i,3}\sigma_3)^2. \tag{24}$$

For some other special distributions of $\Delta\mu_1$, $\Delta\mu_2$ and $\Delta\mu_3$, simple evaluation of $f_{\lambda_i}(z)$ can also be obtained [42].

Based on the definition of PF, given the distribution of $f_{\lambda_i}^{DP}(z)$, we have

$$\begin{aligned} p_f^i &= \text{Prob}(|\lambda_i| > \delta_i \,\big|\, \text{The channel is a DP}) \\ &= 1 - \int_{-\delta_i}^{\delta_i} f_{\lambda_i}^{DP}(z)\, dz. \end{aligned} \tag{25}$$

When μ_1, μ_2 and μ_3 are Gaussian distributed, we can obtain a simple evaluation of p_f^i by

$$\begin{aligned} p_f^i &= 1 - \int_{-\delta_i}^{\delta_i} \frac{1}{2\pi\sigma_{\lambda_i}} \exp\Big(-\frac{z^2}{2\sigma_{\lambda_i}^2}\Big)\, dz \\ &= 2Q\Big(\frac{\delta_i}{\sigma_{\lambda_i}}\Big). \end{aligned} \tag{26}$$

where σ_{λ_i} is given in (24) and $Q(a) = \int_a^\infty \frac{1}{2\pi}\exp\big(-\frac{m^2}{2}\big)\, dm$.

Thus, given a desired value of P_f, the threshold δ_i is computed as

$$\delta_i = Q^{-1}\Big(\frac{P_f}{2}\Big)\sigma_{\lambda_i}, \tag{27}$$

where $Q^{-1}(\bullet)$ is the inverse function of $Q(\bullet)$.

B. Distribution of λ_i in IPs and evaluation of p_d^i

In the case of IP, DOD, DOA and TOA intersect at three intersection points due to both the measurement noise and IP. Particularly, $\bar{\lambda}_i \neq 0$ for IPs.

Let λ_i^{IP} denote λ_i in the case of IPs, and $\bar{\lambda}_i^{IP}$ be the mean value of λ_i^{IP}. According to (16), following similar reasoning of (19) - (23), the probability density function of λ_i^{IP} is

$$f_{\lambda_i}^{IP}(z) = (g_{\Delta\mu_1^i}^{IP} * g_{\Delta\mu_2^i}^{IP} * g_{\Delta\mu_3^i}^{IP})(z), \tag{28}$$

with

$$g_{\Delta\mu_1^i}^{IP}(y) = \frac{1}{|W_{i,1}|} f_{\Delta\mu_1}\Big(\frac{y-\bar{\lambda}_i^{IP}}{W_{i,1}}\Big), \tag{29}$$

$$g_{\Delta\mu_2^i}^{IP}(y) = \frac{1}{|W_{i,2}|} f_{\Delta\mu_2}\Big(\frac{y-\bar{\lambda}_i^{IP}}{W_{i,2}}\Big), \tag{30}$$

$$g_{\Delta\mu_3^i}^{IP}(y) = \frac{1}{|W_{i,3}|} f_{\Delta\mu_3}\Big(\frac{y-\bar{\lambda}_i^{IP}}{W_{i,3}}\Big). \tag{31}$$

where $W_{i,j}$ is the entry of $\mathbf{W}$ in (14) on the ith row and the jth column and $f_{\Delta\mu_1}$, $f_{\Delta\mu_2}$ and $f_{\Delta\mu_3}$ are probability density functions of DOA, DOD and TOA measurement errors, respectively.

Based on the definition of PD, given the distribution of $f_{\lambda_i}^{IP}(z)$,

$$\begin{aligned} p_d^i &= \text{Prob}(|\lambda_i| > \delta_i \,\big|\, \text{The channel is a IP}) \\ &= 1 - \int_{-\delta_i}^{\delta_i} f_{\lambda_i}^{IP}(z)\, dz. \end{aligned} \tag{32}$$

When μ_1, μ_2 and μ_3 are Gaussian distributed with variance σ_1^2, σ_2^2 and σ_3^2, respectively, λ_i^{IP} is also a Gaussian random variable with non-zero mean $\bar{\lambda}_i^{IP}$ and variance $\sigma_{\lambda_i^{IP}}^2 = W_{i,1}^2\sigma_1^2 + W_{i,2}^2\sigma_2^2 + W_{i,3}^2\sigma_3^2$. Then, PD is evaluated by

$$\begin{aligned} p_d^i &= 1 - \int_{-\delta_i}^{\delta_i} \frac{1}{2\pi\sigma_{\lambda_i^{IP}}} \exp\Big(-\frac{(z-\bar{\lambda}_i^{IP})^2}{2\sigma_{\lambda_i^{IP}}^2}\Big)\, dz \\ &= 1 - Q\Big(\frac{-\delta_i - \bar{\lambda}_i^{IP}}{\sigma_{\lambda_i^{IP}}}\Big) + Q\Big(\frac{\delta_i - \bar{\lambda}_i^{IP}}{\sigma_{\lambda_i^{IP}}}\Big). \end{aligned} \tag{33}$$

In conclusion, we note that the averaged (noise-free) intersection points depend on the location of the reflector. We have assumed in our derivation a deterministic location. In practice, such a location cannot be expected to be known. At most, the *distribution* of the reflector locations can be estimated (e.g., uniformly distributed), from which further statistics of PF and PD could be derived.

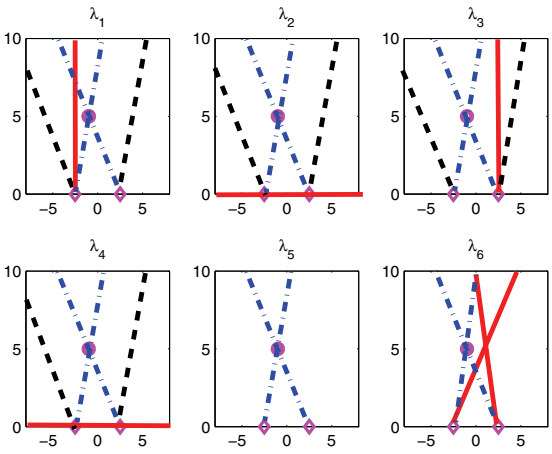

Fig. 4. Illustration of Blind Spots of Different λ_i.

C. Blind Spot of λ_i

There are some situations where the indirect paths can not be effectively detected. Here, we call these special situations "blind spots (BSs)". This subsection studies the BSs for different λ_i.

There are three different kind of situations where the proposed methods do not work well:

- BS1: The reflectors are on the lines of DOD or DOA. In this situation, the DOD and DOA intersection is on the TOA ellipse when no measurement errors exist.
- BS2: The locations of reflectors satisfy any of the three conditions: $\alpha \to 0$, $\beta \to 0$ or $\gamma \to 0$. This is because under these three conditions, $\sigma_{\lambda_i} \to \infty$ according to (24).
- BS3: The locations of reflectors satisfy $\lambda_i \to 0$.

For BS1, the potential locations of reflectors $[m, n]$ satisfy

$$\frac{n}{m-\frac{d}{2}} = \frac{y}{m-\frac{x}{2}} \quad \text{or} \quad \frac{n}{m+\frac{d}{2}} = \frac{y}{m+\frac{x}{2}}, \tag{34}$$

where $[x, y]$ is the location of the target, $[-d/2, 0]$ and $[d/2, 0]$ are the locations of transmitter and receiver, respectively. Given the locations of target and reflectors, the signal can arrive at them through different paths. For simplicity, we consider a reflector location to be BS if the proposed method does not work well for any one of the paths. For example, for transmitter at $[-2.5, 0]$, receiver at $[2.5, 0]$ and target at $[-1, 5]$, the reflector $[-2, \frac{5}{3}]$ is on the line of DOD. The proposed method does not perform well only for the path transmitter-reflector-target-receiver, not the path transmitter-target-reflector-receiver. In this example, we consider the reflector $[-2, \frac{5}{3}]$ to be a BS.

For BS2, the reflectors need to satisfy $\alpha \to 0$, $\beta \to 0$ or $\gamma \to 0$. Particularly, $\alpha \to 0$, which is easy to be satisfied, happens when the DOD is parallel to the DOA.

Table I shows the BS positions for different λ_i. One interesting observation is that BS3 do not exist for λ_5. Note that though we only consider $0 \le \mu_1 \le \pi$ and $0 \le \mu_2 \le \pi$ in this paper, if the full range of μ_1 and μ_2 were considered, a BS3 would be possible, too. One illustration of the BS is shown in Fig. 4, The settings for the illustration are transmitter at $[-2.5, 0]$, receiver at $[2.5, 0]$ and target at $[-1, 5]$.

TABLE I
BLIND SPOTS OF DIFFERENT λ_i

Blind Spots	BS1	BS2	BS3
λ_1	Reflectors satisfying (34)	$\alpha \to 0$ (DOD // DOA), $\beta \to 0$	$\mu_2 = \frac{\pi}{2}$
λ_2	Reflectors satisfying (34)	$\alpha \to 0$ (DOD // DOA), $\beta \to 0$	$\mu_2 = 0$ or π
λ_3	Reflectors satisfying (34)	$\alpha \to 0$ (DOD // DOA), $\gamma \to 0$	$\mu_1 = \frac{\pi}{2}$
λ_4	Reflectors satisfying (34)	$\alpha \to 0$ (DOD // DOA), $\gamma \to 0$	$\mu_1 = 0$ or π
λ_5	Reflectors satisfying (34)	$\beta \to 0$, $\gamma \to 0$	Do not exist
λ_6	Reflectors satisfying (34)	$\beta \to 0$, $\gamma \to 0$	$\mu_1 + \mu_2 = \pi$

It is assumed there is only one reflector $[m, n]$ in the range $m \in [-8, 8] \bigcap n \in [0, 10]$ and the signal propagation path can be either transmitter-reflector-target-receiver, or transmitter-target-reflector-receiver. In the figure, BS1 is shown as blue color dot-dashed lines, BS2 is shown as black color dashed lines and BS3 is shown as red color solid lines. The BS2 of $\beta \to 0$ and $\gamma \to 0$ does not exist in this setting. The BS2 of $\alpha \to 0$ is the black lines which are parallel to the blue lines (DOD and DOA lines). One interesting observation is that λ_5 has the smallest BS: only BS1 exist for λ_5.

For the localization of a target, multiple transmitter-receiver pairs are often used. Different transmitter-receiver pairs have different BSs. Thus, the BSs can be eliminated by combining the IP detection results from multiple transmitter-receiver pairs.

D. "Safe region" and outage probability

In this section, we further study the impact of IPs on target localization, and define the "safe region" and outage probability.

In the previous section, we defined the probability of false alarm as "deciding for a DP whenever an IP actually happens." This has a negative impact on the localization, since IPs add bias to DOD, DOA and TOA measurements, based on which the target is finally localized. However, it can be easily seen that different IPs would have different impact on the localization accuracy . For example, if the non-target reflector is close to the DOD or DOA lines, and adds little bias to DOD, DOA and TOA measurements, then, this IP would have little negative impact on the localization. There are even situations when the reflector does not change the value of DOD, DOA and TOA, e.g., in the case of BS1, the reflector is essentially on the line connecting the transmitter and the target. Thus, the definition of DP or IP does not fully reflect the impact of non-target reflectors on the localization accuracy. To quantify the IPs that do not lead to significant location bias, one could define a region called "safe region", where

$$|\bar{\lambda}_i| < \eta. \tag{35}$$

It is easy to understand that larger value of $|\bar{\lambda}_i|$ leads to less accurate localization. The "safe region" means that in this region, the non-target reflectors have less negative impact on the localization accuracy than reflectors outside this region. Only if the pair of DOD, DOA and TOA is considered to be in "safe region", they are used for localization. The DP can be considered as a special case of "safe region", which has the minimum (no) negative impact on localization accuracy. Given locations of reflectors, the value of $\bar{\lambda}_i$ can be computed, and we can decide whether the path is in "safe region" or not. Moreover, we can define an outage probability of λ_i as follows:

$$\begin{aligned} P^{DP}_{\text{outage},\,i} &= \text{probability}(|\hat{\lambda}_i| > \delta' \,\big|\, |\bar{\lambda}_i| \le \eta_i), \\ P^{IP}_{\text{outage},\,i} &= \text{probability}(|\hat{\lambda}_i| > \delta' \,\big|\, |\bar{\lambda}_i| > \eta_i), \end{aligned} \tag{36}$$

where δ' together with η are the parameters to control the localization accuracy.

There is a tradeoff of choosing the values of δ' and η: with larger values of either δ' or η, IPs are more likely to be considered to be in "safe region", and subsequently used for localization, however, the localization accuracy is decreased by taking more IPs.

V. TDAJ SCHEME WITH NOISY DOD, DOA AND TOA

In this section, we discuss the computation of threshold δ_i given a required PF. Then, the procedures of TDAJ is presented.

According to (23), if we perfectly know the value of $f^{DP}_{\lambda_i}$, the value of δ_i can be reversely computed to achieve a given PF. However, $f^{DP}_{\lambda_i}$ depends on $f_{\Delta\mu_1}(\bullet)$, $f_{\Delta\mu_2}(\bullet)$ and $f_{\Delta\mu_3}(\bullet)$ which are known and the values of $W_{i,1}$, $W_{i,2}$ and $W_{i,3}$ which are not accurately known. Thus, the values of $W_{i,1}$, $W_{i,2}$ and $W_{i,3}$ have to be estimated based on the measurements of DOA $\hat{\mu}_1$, DOD $\hat{\mu}_2$ and TOA $\hat{\mu}_3$.

The procedure of TDAJ is listed in Algorithm 1:

Algorithm 1 DOD, DOA and TOA joint (TDAJ) IP Detection Scheme

1. Compute the three intersections $[\hat{x}_1, \hat{y}_1]$, $[\hat{x}_2, \hat{y}_2]$ and $[\hat{x}_3, \hat{y}_3]$ from DOA, DOD and TOA measurements $\hat{\mu_1}$, $\hat{\mu_2}$ and $\hat{\mu}_3$.
2. Compute the matrix $\mathbf{W}$ based on (11) and (14) using the values of $[\hat{x}_1, \hat{y}_1]$, $[\hat{x}_2, \hat{y}_2]$ and $[\hat{x}_3, \hat{y}_3]$ from Step 1.
3. Then, calculate the distribution of $f^{DP}_{\lambda_i}(z)$ according to (20) - (23).
4. Reversely compute the value of δ_i given P_f by (27).
5. Compare the value of six difference observations of λ_i from (5) with threshold δ_i, $(i = 1, 2, ..., 6)$ and perform IP detection based on individual rule (7) or fusion rule (4).

VI. SIMULATION RESULTS

In this section, extensive simulations are employed to verify the theoretical results, evaluate the performance of TDAJ algorithms and test the improvement of localization accuracy by IP detection.

TABLE II
SIMULATION PARAMETERS

	P_t^{dB}	Target Location	Reflector Location
Scenario 1	1 dBm	fixed at [5.2, 10]	[4.8, 9.8]
Scenario 2	1 dBm	fixed at [5.2, 10]	Uniformly distributed at $x \in [-8,8] \bigcap y \in [0,10]$
Scenario 3	1 dBm	The target and one reflector are uniformly distributed at $x \in [-8,8] \bigcap y \in [0,10]$	
Scenario 4	25 dBm	The target and two reflectors are uniformly distributed at $x \in [-8,8] \bigcap y \in [0,10]$	
Scenario 5	Changing	The target and one reflector are uniformly distributed at $x \in [-8,8] \bigcap y \in [0,10]$	

A. Simulation Description

There are 6 scenarios considered for the simulation, and the parameters of them are shown in Table II. In scenario 1, the radio propagation path is designed as transmitter-reflector-target-receiver; in scenario 2 and 3, the sequence of signal arrival at target/reflectors is random: the signal propagation path is either transmitter-target-reflector-receiver or transmitter-reflector-target-receiver with equal probability; in scenario 4 and 5, the signal propagation path is transmitter-object1-object2-object3-receiver, and the target and two receivers are randomly assigned to the three objects.

In all scenarios, the transmitter and receiver are at $[-2.5, 0]$ and $[2.5, 0]$, respectively. In this paper, we assume the locations of all objects (transmitter, target, etc.) are in meters. The measurement errors for μ_i are Gaussian, and the standard deviation of them (σ_i, $i = 1, 2, 3$) are given in meters or degrees, respectively. The values of σ_i, which are dependent of the target and reflector locations, are chosen as follows.

First, we employ a signal power loss model commonly used in the radar community [43], [44]. We assume the noise power spectral density is -174 dBm/Hz, the carrier frequency is 3 GHz, and the bandwidth of the signal is 1 GHz. The noise power is $P_n^{dB} = -174 + 10\log_{10}(10^9) = -84$ dBm. Assuming that the wireless signal is reflected by the target and H non-target reflectors, the signal transmission path is divided into $H + 2$ sub-paths[2]. As an example shown in Fig. 1, there are two sub-paths p_1 and p_2 for a DP, and three sub-paths p_1, p_3 and p_4 for an IP. We let p_h be the length of the hth ($h = 1, 2, ..., H + 2$) sub-path. The free space path loss through hth sub-path is evaluated by

$$L_h^{dB} = -10\log_{10}(4\pi p_h^2)$$

Let the transmitted signal power in dB be P_t^{dB}, the signal-to-noise radio (SNR) in dB may be evaluated as follows [43], [44]:

$$\begin{aligned} \text{SNR} &= P_t^{dB} - P_n^{dB} + G_{TX}^{dB} + 10\log_{10}(A_{RX}) + \\ &\quad \sum_{h=1}^{H+2} L_h^{dB} + 10\log_{10}(R_t R_r^H) \qquad (37) \\ &= P_t^{dB} + 88 - \sum_h 10\log_{10}(4\pi p_h^2) - 0.22H, \end{aligned}$$

where $G_{TX}^{dB} = 15$ dB is the transmitter gain in dB, $A_{RX} = 0.0796$ is the receiver antenna aperture, $R_t = 1$ m^2 is the radio cross section (RCS) for the target, and $R_r = 0.95$ m^2 is the RCS for any non-target reflectors.

[2]We assume the signal is only reflected once by target and non-target reflectors

TABLE III
P_f AND P_d OF INDIVIDUAL RULES BASED ON λ_1, λ_3, λ_5 FOR SCENARIO 1

Expected P_f		0.05	0.1	0.3	0.5	0.9	0.95
λ_1	Simulated P_f	0.050	0.100	0.296	0.495	0.898	0.949
	P_d by (33)	0.570	0.689	0.865	0.931	0.990	0.995
	Simulated P_d	0.576	0.700	0.876	0.938	0.991	0.995
λ_3	Simulated P_f	0.049	0.100	0.297	0.495	0.898	0.949
	P_d by (33)	0.542	0.663	0.849	0.921	0.988	0.994
	Simulated P_d	0.549	0.683	0.872	0.937	0.991	0.995
λ_5	Simulated P_f	0.050	0.100	0.296	0.496	0.898	0.949
	P_d by (33)	0.593	0.709	0.877	0.938	0.991	0.995
	Simulated P_d	0.595	0.711	0.878	0.939	0.991	0.995

Second, we model the standard deviations of DOA (σ_1), DOD (σ_2) to be proportional to the square root of the Cramer Rao Lower Bounds (CRLBs) [45], [46] :

$$\sigma_1 = \frac{1}{2}\sqrt{\frac{6}{\text{SNR}N_{ar}(N_{ar}^2-1)}}\frac{1}{\sin\bar{\mu}_1} = \frac{0.05}{\sin\bar{\mu}_1\sqrt{\text{SNR}}}, \quad (38)$$

$$\sigma_2 = \frac{1}{2}\sqrt{\frac{6}{\text{SNR}N_{ar}(N_{ar}^2-1)}}\frac{1}{\sin\bar{\mu}_2} = \frac{0.05}{\sin\bar{\mu}_2\sqrt{\text{SNR}}}. \quad (39)$$

where $\bar{\mu}_1$ and $\bar{\mu}_2$ are the mean values of DOA and DOD.

The standard deviation of the TOA estimate σ_3 is assumed to be [3]

$$\sigma_3 = \frac{\varpi}{\pi\sqrt{\text{SNR}}} = \frac{0.038}{\sqrt{\text{SNR}}}. \quad (40)$$

To test whether our model of σ_i is consistent with practical results [40], we consider a DP with a target at $[7.8, 14]$ and the transmitter power $P_t^{dB} = 1$ dBm. Then we can compute SNR $= 18.71$ dB, $\sigma_1 = 0.36$ degree, $\sigma_2 = 0.41$ degree and $\sigma_3 = 0.0044$ meter. The values of σ_i are consistent with the results in [38]–[40]. In the simulation of every scenario, $2{*}10^5$ samples are collected. For every sample, the estimates of μ_i ($i = 1, 2, 3$) are Gaussian random variables with σ_i computed according to (38) - (40).

B. Comparison between theoretical and simulated PF and PD

The performances TDAJ for Scenario 1 based on λ_1, λ_3, λ_5 are listed in Table III. According to the definition in (7), PF is computed as the probability of claiming an IP when there are no reflectors and PD is computed as the probability of claiming an IP when there are reflectors. The expected PF, PD computed by (33), PF and PD by simulations are shown. From the results, we can observe that:

- The TDAJ scheme based on λ_i can closely approximate the expected PF,
- The closed-form evaluation of PD by (33) is consistent with PD obtained from simulations.

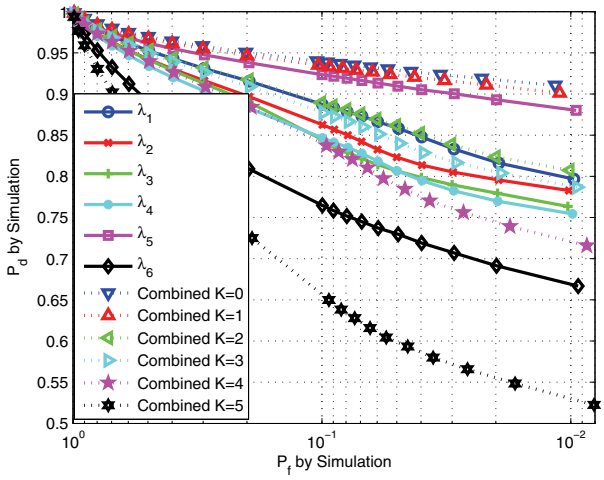

Fig. 5. P_d vs P_f in Scenario 2.

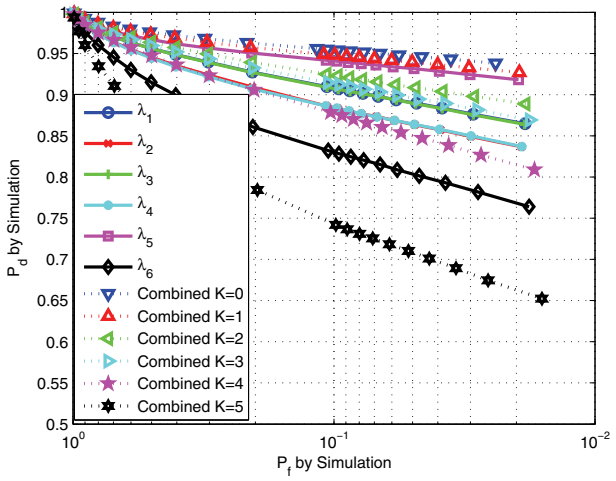

Fig. 6. P_d vs P_f in Scenario 3.

TABLE IV
P_f AND P_d OF FOR SCENARIO 2

Expected P_f		0.03	0.04	0.05	0075	0.1
P_f	λ_5	0.0294	0.0397	0.0496	0.0691	0.0998
	FR ($K=0$)	0.0334	0.0439	0.0544	0.0743	0.1049
	FR ($K=5$)	0.0260	0.0357	0.0452	0.0640	0.0938
P_d	λ_5	0.9002	0.9051	0.9095	0.9164	0.9234
	FR ($K=0$)	0.9237	0.9272	0.9302	0.9348	0.9400
	FR ($K=5$)	0.5657	0.5799	0.5933	0.6157	0.6499

C. Comparison of IP Detection Performance by Different λ_i

The simulated PD vs. PF curves for Scenario 2 - 4 are drawn in Fig. 5 to Fig. 7, respectively. It can be observed that

- In common UWB localization systems (Scenario 2 - 4), the TDAJ can very accurately detect the IP, e.g., $P_f < 10\%$ and $P_d > 90\%$.
- The TDAJ scheme based on λ_5 has the best performance among individual rules in the sense that it accurately achieves the expected PF and maximizes the PD. This is because λ_5 has fewer BSs than others, as discussed in Section IV. C.

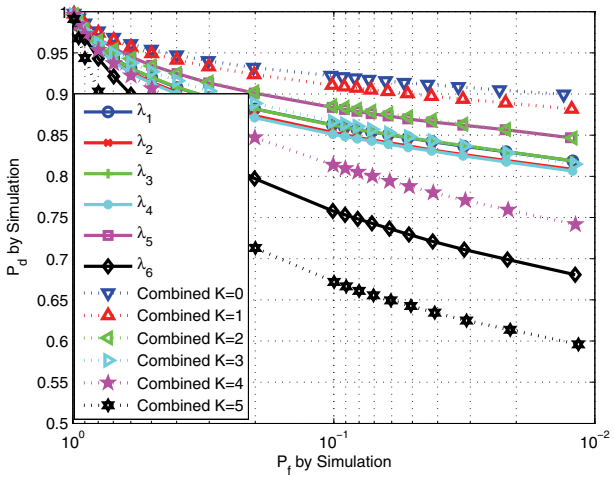

Fig. 7. P_d vs P_f in Scenario 4.

In Table IV, we list the the PF and PD of the individual rule λ_5 and fusion rule (FR) with $K=0$ and $K=5$ for scenario 2, which shows that FR with $K=0$ and $K=5$ achieve a little higher and lower PF than the expected one, while individual rule based on λ_5 accurately achieves the expected PF. This is because when the model for the λ_i is imperfect (the reasons for the imperfect model are analyzed in Section VI. D), the decisions from the different λ_i are not perfectly correlated. Consequently, we might obtain a false alarm from some λ_i but not others. In that case, we can conclude that a "fusion rule" with $K=0$ has a larger P_f than a decision rule based on a single λ_i, since *any* λ_i deciding for a P_f leads to an overall decision for P_f. Conversely, a fusion rule with $K=5$ will lead to a smaller P_f than the individual decision rules, since *every* λ_i must claim a P_f.

D. PF and PD vs. Transmitted Signal Power

In Scenario 5, we study the impact of transmitted signal power P_t^{dB}. High P_t^{dB} leads to smaller standard deviation of DOA, DOD and TOA estimates, and consequently better IP detection performance. The simulated PD and PF vs. P_t^{dB} are shown in Fig. 8, with expected PF $= 5\%$.

From Scenario 5, we can observe that an increasing transmitted signal power improves the TDAJ performances: closer to expected PF and higher PD. In terms of PF, TDAJ based on λ_5 is less impacted by the increase of the error level than the Fusion Rule (FL) with $K=0$ and $K=1$. Even with $P_t^{dB} = -5$ dBm, TDAJ based on λ_5 can achieve $P_f = 5\%$ and $P_d > 85\%$.

The main reasons for inaccurate PF and decreasing PD with high level of errors are:

1) The linear relations between Δx, Δy and μ_1, μ_2 and μ_3 (9) are not valid.
2) The threshold δ calculated based on noisy measurements μ_1, μ_2 and μ_3 is not accurate.

E. Improvement of Localization by IP Detection

In this section, we examine the improvement of localization accuracy by the IP detection. For the localization, the final

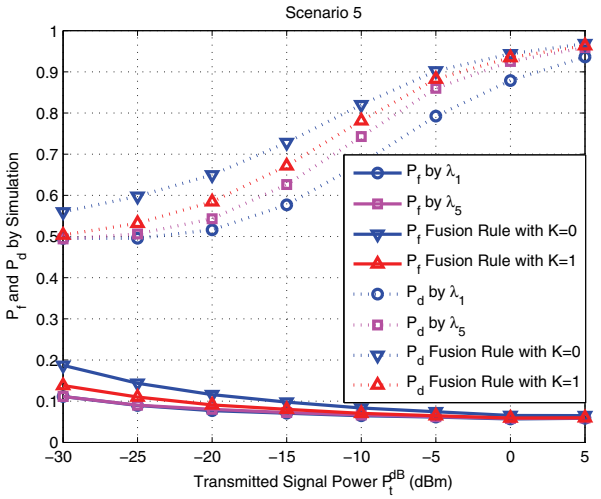

Fig. 8. P_d and P_f vs transmitted signal power P_t^{dB} (dBm) in Scenario 5

estimate of the target location is obtained based on the maximum likelihood (ML) estimation. The ML estimation is performed by a Quasi-Gaussian iterative method [47], with the initial value being the average of the three intersections (DOA/DOD, DOA/TOA and DOD/TOA).

In the simulation, we consider the problem of localization in an indoor environment with range $x \in [-5,5] \bigcap y \in [0,8]$. There are totally $2 * 10^5$ samples. The errors of DOA, DOD and TOA estimates are generated based on the model in (38) - (40). In 10^5 samples, there is no reflector, and in the remaining 10^5 samples, there is one reflector uniformly distributed in the region $x \in [-5,5] \bigcap y \in [0,8]$. The transmitter and receiver are at $[-2.5, 0]$ and $[2.5, 0]$, respectively. The target location is shown in Table V. Two localization strategies are simulated and compared, the first one is without IP detection but checking whether the average of three intersection $[\frac{\hat{x}_1+\hat{x}_2+\hat{x}_3}{3}, \frac{\hat{y}_1+\hat{y}_2+\hat{y}_3}{3}]$ in the in the region $x \in [-5,5] \bigcap y \in [0,8]$. If the average of three intersections is inside the region, for any triplet of DOD, DOA and TOA, the localization is performed. The second one is to first perform IP detection, and only when the triplet is considered to be DP based on the individual rule with λ_5, the localization is performed. The root mean square error (RMSE) is utilized to evaluate the localization accuracy, which is defined by

$$\text{RMSE} = \sqrt{\text{Mean}\left(\left(\hat{x}_{RMSE} - \bar{x}\right)^2 + \left(\hat{y}_{RMSE} - \bar{y}\right)^2\right)} \quad (41)$$

where $[\bar{x}, \bar{y}]$ is the true target location and $[\hat{x}_{RMSE}, \hat{y}_{RMSE}]$ is the ML estimate of target location using the Quasi-Gaussian iterative method.

Table V shows the values of RMSE without IP detection, RMSE with IP detection, PF and PD for several target locations. It can be observed that the IP detection can increase the localization accuracy by several orders of magnitude.

VII. Conclusion

This paper studied the problem of discriminating IPs and DPs for passive positioning purposes, from a novel perspective. We utilize the TOA, DOD and DOA information together and test whether the parameter tuplet is consistent with the assumption of a DP. In particular, we test the differences of the three intersections from DOD, DOA and TOA measurements λ_i $(i = 1, 2, ..., 6)$ for IP detection. The algorithm is based on Neyman-Pearson criteria to maximize the probability of detection given probability of false alarm. Several individual rules and fusion rules under this framework are discussed. The "blind spots" of individual rules are investigated and it is shown that λ_5 has the smallest "blind spots". Simulations show that the algorithm can effectively detect IPs when the TOA, DOD and DOA measurements are available with small errors. As verified by simulations, the proposed method can be employed to sort out DPs to increase localization accuracy. Furthermore, the identified DPs can also be used for other purposes such as generation of environmental maps.

TABLE V
Localization RMSE Comparison

Target Location	$[-1, 5]$	$[-2, 6]$	$[3, 7]$	$[-3, 4.6]$
RMSE without IP Detection	4.2575	5.4581	4.2980	4.6665
RMSE with IP Detection	0.5602	0.8152	0.7863	0.5179
PF	0.0504	0.0498	0.0506	0.0496
PD	0.9832	0.9806	0.9760	0.9797

VIII. Acknowledgements

We thank Dr. S. Niranjayan for many helpful discussions. Part of this work was supported by the Office of Naval Research (ONR) under grant 10599363. The opinions expressed in this paper are those of the authors and need not reflect those of ONR.

Appendix
Proof of Theorem 1

Since in the case of DP, we have $a_j = a_j^k$, $b_j = b_j^k$ and $c_j = c_j^k$ for $j = 1, 2, 3$. With some manipulations, we can rewrite $\mathbf{W}$ in (14) as

$$\mathbf{W} = \begin{bmatrix} -\frac{c_1 b_2}{\alpha^{DP}} & -\frac{b_2 c_2 \gamma^{DP}}{\alpha^{DP}\beta^{DP}} & -\frac{b_2 c_3}{\beta^{DP}} \\ \frac{a_2 c_1}{\alpha^{DP}} & \frac{a_2 c_2 \gamma^{DP}}{\alpha^{DP}\beta^{DP}} & \frac{a_2 c_3}{\beta^{DP}} \\ \frac{b_1 c_1 \beta^{DP}}{\alpha^{DP}\gamma^{DP}} & \frac{b_1 c_2}{\alpha^{DP}} & \frac{b_1 c_3}{\gamma^{DP}} \\ -\frac{a_1 c_1 \beta^{DP}}{\alpha^{DP}\gamma^{DP}} & -\frac{a_1 c_2}{\alpha^{DP}} & -\frac{a_1 c_3}{\gamma^{DP}} \\ -\frac{b_3 c_1}{\gamma^{DP}} & -\frac{b_3 c_2}{\beta^{DP}} & -\frac{b_3 c_3 \alpha^{DP}}{\beta^{DP}\gamma^{DP}} \\ \frac{a_3 c_1}{\gamma^{DP}} & \frac{a_3 c_2}{\beta^{DP}} & \frac{a_3 c_3 \alpha^{DP}}{\beta^{DP}\gamma^{DP}} \end{bmatrix}. \quad (42)$$

where

$$\begin{aligned} \alpha^{DP} &= a_1 b_2 - a_2 b_1, \\ \beta^{DP} &= a_2 b_3 - a_3 b_2, \\ \gamma^{DP} &= a_3 b_1 - a_1 b_3. \end{aligned}$$

Then, it follows that for $i = 1, 2, ..., 6$,

$$\begin{aligned} W_{1,i} &= -\frac{b_2}{a_2} W_{2,i} = -\frac{b_2 \gamma^{DP}}{b_1 \beta^{DP}} W_{3,i} = \frac{b_2 \gamma^{DP}}{a_1 \beta^{DP}} W_{4,i} \quad (44) \\ &= \frac{b_2 \gamma^{DP}}{b_3 \alpha^{DP}} W_{5,i} = -\frac{b_2 \gamma^{DP}}{a_3 \alpha^{DP}} W_{6,i}. \end{aligned}$$

According to (13),

$$\hat{\boldsymbol{\lambda}}^{DP} = \boldsymbol{\varepsilon} = \mathbf{W} \Delta \boldsymbol{\mu}.$$

where $\boldsymbol{\Delta\mu}$ is defined in (15). Thus, we have

$$\begin{aligned}\hat{\lambda}_1^{DP} &= -\frac{b_2}{a_2}\hat{\lambda}_2^{DP} = -\frac{b_2\gamma^{DP}}{b_1\beta^{DP}}\hat{\lambda}_3^{DP} = \frac{b_2\gamma^{DP}}{a_1\beta^{DP}}\hat{\lambda}_4^{DP} \quad (45)\\ &= \frac{b_2\gamma^{DP}}{b_3\alpha^{DP}}\hat{\lambda}_5^{DP} = -\frac{b_2\gamma^{DP}}{a_3\alpha^{DP}}\hat{\lambda}_6^{DP}.\end{aligned}$$

which finishes the proof.

REFERENCES

[1] J. Shen and A. F. Molisch, "Indirect path detection of passive localization based on wireless propagation measurements," in *2012 IEEE International Conference on Ultra-Wideband*.

[2] S. Gezici, Z. Tian, G. Giannakis, H. Kobayashi, A. F. Molisch, H. Poor, and Z. Sahinoglu, "Localization via ultra-wideband radios: a look at positioning aspects for future sensor networks," *IEEE Signal Process. Mag.*, vol. 22, no. 4, pp. 70–84, July 2005.

[3] D. Dardari, A. Conti, U. Ferner, A. Giorgetti, and M. Win, "Ranging with ultrawide bandwidth signals in multipath environments," *Proc. IEEE*, vol. 97, no. 2, pp. 404–426, Feb. 2009.

[4] M. Kuhn, C. Zhang, B. Merkl, D. Yang, Y. Wang, M. Mahfouz, and A. Fathy, "High accuracy UWB localization in dense indoor environments," in *Proc. 2008 IEEE International Conference on Ultra-Wideband*, vol. 2, pp. 129–132.

[5] S. Gezici and H. Poor, "Position estimation via ultra-wide-band signals," *Proc. IEEE*, vol. 97, no. 2, pp. 386–403, Feb. 2009.

[6] Y. Shen and M. Win, "Fundamental limits of wideband localization—part I: a general framework," *IEEE Trans. Inf. Theory*, vol. 56, no. 10, pp. 4956–4980, Oct. 2010.

[7] Y. Shen, H. Wymeersch, and M. Win, "Fundamental limits of wideband localization—part II: cooperative networks," *IEEE Trans. Inf. Theory*, vol. 56, no. 10, pp. 4981–5000, Oct. 2010.

[8] J. Zhang, P. Orlik, Z. Sahinoglu, A. F. Molisch, and P. Kinney, "UWB systems for wireless sensor networks," *Proc. IEEE*, vol. 97, no. 2, pp. 313–331, 2009.

[9] M. Win, A. Conti, S. Mazuelas, Y. Shen, W. Gifford, D. Dardari, and M. Chiani, "Network localization and navigation via cooperation," *IEEE Commun. Mag.*, vol. 49, no. 5, pp. 56–62, May 2011.

[10] A. Tajer, G. Jajamovich, X. Wang, and G. Moustakides, "Optimal joint target detection and parameter estimation by MIMO radar," *IEEE J. Sel. Topics Signal Process.*, vol. 4, no. 1, pp. 127–145, 2010.

[11] E. Paolini, A. Giorgetti, M. Chiani, R. Minutolo, and M. Montanari, "Localization capability of cooperative anti-intruder radar systems," *EURASIP J. Advances in Signal Process.*, vol. 2008, no. 17, 2008.

[12] A. Haimovich, R. Blum, and L. Cimini, "MIMO radar with widely separated antennas," *IEEE Signal Process. Mag.*, vol. 25, no. 1, pp. 116–129, 2008.

[13] M. Klemm, J. Leendertz, D. Gibbins, I. Craddock, A. Preece, and R. Benjamin, "Microwave radar-based differential breast cancer imaging: imaging in homogeneous breast phantoms and low contrast scenarios," *IEEE Trans. Antennas Propag.*, vol. 58, no. 7, pp. 2337–2344, July 2010.

[14] J.-Y. Lee and R. Scholtz, "Ranging in a dense multipath environment using an UWB radio link," *IEEE J. Sel. Areas Commun.*, vol. 20, no. 9, pp. 1677–1683, Dec. 2002.

[15] K. Pahlavan, F. O. Akgul, M. Heidari, A. Hatami, J. M. Elwell, and R. D. Tingley, "Indoor geolocation in the absence of direct path," *IEEE Wireless Commun.*, vol. 13, no. 6, pp. 50–58, 2006.

[16] B. Alavi and K. Pahlavan, "Modeling of the TOA-based distance measurement error using UWB indoor radio measurements," *IEEE Commun. Lett.*, vol. 10, no. 4, pp. 275–277, Apr. 2006.

[17] J. Khodjaev, Y. Park, and A. Saeed Malik, "Survey of NLOS identification and error mitigation problems in UWB-based positioning algorithms for dense environments," *Annals of Telecommun.*, vol. 65, no. 5, pp. 301–311, 2010.

[18] L. Cong and W. Zhuang, "Non-line-of-sight error mitigation in TDOA mobile location," in *Proc. 2001 IEEE Global Telecommunications Conference*, vol. 1, pp. 680–684.

[19] M. McGuire and K. Plataniotis, "Dynamic model-based filtering for mobile terminal location estimation," *IEEE Trans. Veh. Technol.*, vol. 52, no. 4, pp. 1012–1031, 2003.

[20] L. Cong and W. Zhuang, "Nonline-of-sight error mitigation in mobile location," *IEEE Trans. Wireless Commun.*, vol. 4, no. 2, pp. 560–573, 2005.

[21] K. Yu and Y. Guo, "Improved positioning algorithms for nonline-of-sight environments," *IEEE Trans. Veh. Technol.*, vol. 57, no. 4, pp. 2342–2353, 2008.

[22] M. kyoung Kang, J. Kang, S. W. Lee, Y.-J. Park, and K. H. Kim, "NLOS mitigation for low-cost IR-UWB RTLS," in *2011 IEEE International Conference on Ultra-Wideband*.

[23] A. Conti, M. Guerra, D. Dardari, N. Decarli, and M. Win, "Network experimentation for cooperative localization," *IEEE J. Sel. Areas Commun.*, vol. 30, no. 2, pp. 467–475, Feb. 2012.

[24] I. Guvenc, C.-C. Chong, F. Watanabe, and H. Inamura, "NLOS identification and weighted least-squares localization for UWB systems using multipath channel statistics," *EURASIP J. Adv. Signal Process.*, Jan. 2008.

[25] A. Maali, H. Mimoun, G. Baudoin, and A. Ouldali, "A new low complexity NLOS identification approach based on UWB energy detection," in *Proc. 2009 IEEE Radio and Wireless Symposium*, pp. 675–678.

[26] I. Guvenc and C.-C. Chong, "A survey on TOA based wireless localization and NLOS mitigation techniques," *IEEE Commun. Surveys & Tutorials*, vol. 11, no. 3, pp. 107–124, 2009.

[27] K. Yu and Y. Guo, "Statistical NLOS identification based on AOA, TOA, and signal strength," *IEEE Trans. Veh. Technol.*, vol. 58, no. 1, pp. 274–286, 2009.

[28] N. Alsindi, C. Duan, J. Zhang, and T. Tsuboi, "NLOS channel identification and mitigation in ultra wideband ToA-based wireless sensor networks," in *Proc. 2009 Workshop on Positioning, Navigation and Communication*, pp. 59–66.

[29] S. Marano and, W. M. Gifford, H. Wymeersch, and M. Z. Win, "NLOS identification and mitigation for localization based on UWB experimental data," *IEEE J. Sel. Areas Commun.*, vol. 28, no. 7, pp. 1026–1035, 2010.

[30] N. Decarli, D. Dardari, S. Gezici, and A. A. D'Amico, "LOS/NLOS detection for UWB signals: a comparative study using experimental data," in *Proc. 2010 IEEE International Symposium on Wireless Pervasive Computing*, pp. 169–173.

[31] B. Fleury, M. Tschudin, R. Heddergott, D. Dahlhaus, and K. Ingeman Pedersen, "Channel parameter estimation in mobile radio environments using the SAGE algorithm," *IEEE J. Sel. Areas Commun.*, vol. 17, no. 3, pp. 434–450, Mar. 1999.

[32] A. Richter, "Estimation of radio channel parameters: models and algorithms," Ph.D. dissertation, Technischen Universität Ilmenau, Germany, May 2005, ISBN 3-938843-02-0.

[33] J. Salmi and A. F. Molisch, "Propagation parameter estimation, modeling and measurements for ultrawideband MIMO radar," *IEEE Trans. Antennas Propag.*, vol. 59, no. 11, pp. 4257–4267, Nov. 2011.

[34] A. F. Molisch, *Wireless Communications*, 2nd edition. Wiley, 2011.

[35] Y. Shen and M. Win, "On the accuracy of localization systems using wideband antenna arrays," *IEEE Trans. Commun.*, vol. 58, no. 1, pp. 270–280, Jan. 2010.

[36] J. Shen and A. F. Molisch, "Discerning direct and indirect paths: principle and application in passive target positioning systems," in *Proc. 2011 IEEE Global Telecommunications Conference*, pp. 1–6.

[37] I. Chahbi and B. Jouaber, "A joint AOA, AOD and delays estimation of multipath signals based on beamforming techniques," in *Proc. 2010 Asilomar Conference on Signals, Systems and Computers*, pp. 603–607.

[38] J. Shen and A. F. Molisch, "Passive location estimation using TOA measurements," in *2011 IEEE International Conference on Ultra-Wideband*.

[39] J. Shen, A. F. Molisch, and J. Salmi, "Accurate passive location estimation using TOA measurements," *IEEE Trans. Wireless Commun.*, vol. 11, no. 6, pp. 2182–2192, June 2012.

[40] L. Taponecco, A. D'Amico, and U. Mengali, "Joint TOA and AOA estimation for UWB localization applications," *IEEE Trans. Wireless Commun.*, vol. 10, no. 7, pp. 2207–2217, July 2011.

[41] S. M. Kay, *Fundamentals of Statistical Signal Processing*. Prentice-Hall, Inc., 1993.

[42] C. M. Grinstead and J. L. Snell, *Introduction to Probability*. American Mathematical Society, 1997.

[43] C. Wolff, "Radar tutorial," 2011. Available: http://www.radartutorial.eu/druck/Book1.pdf

[44] S. Kingsley and S. Quegan, *Understanding Radar Systems*. SciTech Publishing, 1999.

[45] A. Mirkin and L. Sibul, "Cramer-Rao bounds on angle estimation with a two-dimensional array," *Trans. Signal Process.*, vol. 39, no. 2, pp. 515–517, Feb. 1991. Available: http://dx.doi.org/10.1109/78.80843

[46] R. Adve, "Direction of arrival estimation." Available: http://www.comm.toronto.edu/~rsadve/Notes/DOA.pdf

[47] D. F. Shanno, "Conditioning of quasi-Newton methods for function minimization," *Mathematics of Computation*, vol. 24, no. 111, pp. 647–656, 1970.

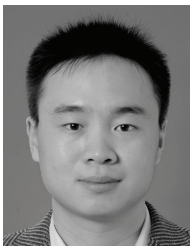

Junyang Shen (S'08) received the B.S. degree from Huazhong University of Science and Technology, China, in 2006 and the M.S. degree (Hon.) from Beijing University of Posts and Technology, China, in 2009. Since Aug. 2009, he worked toward the Ph.D. degree with the Department of Electrical and Engineering, University of Southern California, Los Angeles. He has researched on spectrum sensing in Cognitive Radio. Now, His research interests cover MIMO radar, UWB location and monitoring. He has served as a Technical Program Committee (TPC) member for the IEEE International Conference on Communications (ICC) in 2012. He received the Best Student Paper Award in IEEE International Conference on Ultra-Wideband (ICUWB), 2011.

Andreas F. Molisch (S'89, M'95, SM'00, F'05) is Professor of Electrical Engineering at the University of Southern California, Los Angeles, CA, USA. Previously, he was with AT&T (Bell) Laboratories Research (USA), Lund University (Sweden), Mitsubishi Electric Research Labs, (USA), and TU Vienna (Austria).

Dr. Molisch's current research interests are measurement and modeling of mobile radio channels, UWB communications and localization, cooperative communications, MIMO systems, advanced cellular architectures, and wireless systems for healthcare. He has authored, coauthored or edited four books, among them the textbook *Wireless Communications* (Wiley-IEEE Press), 14 book chapters, more than 140 journal papers, and numerous conference contributions, as well as more than 70 patents and 60 standards contributions.

Dr. Molisch has been an editor of a number of journals and special issues, General Chair, TPC Chair, or Symposium Chair of multiple international conferences, and chairman of various international standardization groups. He is a Fellow of the IEEE, a Fellow of the IET, an IEEE Distinguished Lecturer, and a member of the Austrian Academy of Sciences. He is the recipient of numerous awards, most recently the Donald Fink Prize of the IEEE and the Eric Sumner Award of the IEEE.